

ARTICLE OPEN

Building egg-tray-shaped graphenes that have superior mechanical strength and band gap

Wei Liu^{1,2,3}, Lei Zhao^{4,5}, Eva Zurek⁶, Jing Xia³, Yong-hao Zheng⁵, Hai-qing Lin¹, Jing-yao Liu⁷ and Mao-sheng Miao^{4,1}

The major hindrances of implementing graphene in two-dimensional (2D) electronics are both mechanical (the tendency to crumble and form ripples) and electrical (the lack of a band gap). Moreover, the inevitable structural defects in graphene have a profound influence on its physical and chemical properties. Here, we propose a family of 2D egg-tray graphenes constructed by arranging pentagon and heptagon defects in the graphene lattice based on a careful analysis of the topological distribution of minima, maxima, and saddle points. First-principles calculations show that the egg-tray graphenes are dynamically stable, and their energies, which depend on the concentration of pentagons and heptagons, are the lowest among carbon allotropes. These 2D carbon allotropes exhibit a large variation in their electronic properties, ranging from semimetallic to semiconducting, including some allotropes that have Dirac cones in their band structures. Furthermore, some egg-tray graphenes are predicted to have negative Poisson's ratios. The adsorption of Li atoms on the egg-tray graphenes is considerably stronger than the adsorption on perfect graphene, therefore they may absorb Li more effectively than graphene, which is important for improving the performance of rechargeable Li batteries.

npj Computational Materials (2019)5:71; <https://doi.org/10.1038/s41524-019-0211-2>

INTRODUCTION

Graphene has become a superstar in both academia and industry, ever since its discovery in 2004.^{1–3} Perfect graphene is a one-atom-thick layer of sp^2 carbon atoms arranged in a honeycomb lattice, and it has shown many outstanding properties such as the room-temperature Hall effect,⁴ ambipolar field effect,¹ exceptional carrier mobility,^{5–7} and high thermal conductivity,⁸ etc. However, structural defects inevitably appear during the growth or processing of graphene, and these defects strongly influence graphene's physical and chemical properties by breaking its perfect symmetry. For example, the presence of defects significantly reduces the mobility of charge carriers, thus increasing the resistivity of graphene,^{9,10} which weakens the performance of graphene-based devices. On the other hand, some studies have shown that structural defects can locally increase the reactivity of graphene and provide adsorption sites for atoms or molecules, which is very important for the catalytic applications of graphene. The applications of pristine graphene in nanoscale electronic devices are strongly limited by the fact that it has a zero band gap. Therefore, many different ways that can open a band gap in graphene-based materials have been proposed, and the introduction of defects in the graphene lattice has been demonstrated to be an effective way to tune the electronic properties of graphene.^{11,12}

The graphene lattice has the unique ability to incorporate structural defects by reconstructing carbon atoms into nonhexagonal rings. The simplest example is the Stone–Wales defect,¹³ in which four hexagons are converted into two pentagons and two

heptagons by rotating one C–C bond by 90°. In addition, tetragons, octagons, and larger carbon rings have been reported in graphene.^{11,14,15} These nonhexagonal rings are expected to dramatically alter both the structures and properties of graphene.^{15,16} Since the discovery of the fullerenes, it has been known that the inclusion of certain types of nonhexagonal rings in its planar hexagonal network will induce local Gaussian curvature. The insertion of one pentagon into the graphene sheet will produce a surface with positive Gaussian curvature, namely a carbon nanocone, which has been predicted to be a promising candidate as a phononic device and electronic sensor.^{17–19} On the other hand, the presence of one heptagon or octagon in the graphene sheet will lead to a negatively curved surface, which is a structural feature that is desirable for applications in alkali-ion batteries.²⁰ Hence, considering the important structure–property relationships in carbon allotropes, it is necessary to systematically study systems with different arrangements of these nonhexagonal rings in the graphene lattice. Knowing how structural defects impact properties will enable the rational design of new graphene-based materials for a wide variety of future applications.

In this work, we propose a strategy to study the arrangement of structural defects in the graphene lattice. By arranging nonhexagonal rings in the graphene lattice according to topological diagrams, we obtain a series of two-dimensional (2D) carbon allotropes possessing hillocks and trenches. Their thermodynamic stability as well as electronic and mechanical properties is thoroughly investigated using first-principles calculations. The results show that the topological arrangement of the

¹Beijing Computational Science Research Center, 100193 Beijing, PR China; ²Department of Optical Engineering, Zhejiang A & F University, Lin'an 311300 Zhejiang, PR China; ³Department of Physics and Astronomy, University of California, Irvine, CA 92697, USA; ⁴Department of Chemistry & Biochemistry, California State University, Northridge, CA 91330-8262, USA; ⁵School of Optoelectronic Science and Engineering, University of Electronic Science and Technology of China (UESTC), 610054 Chengdu, PR China; ⁶Department of Chemistry, State University of New York at Buffalo, Buffalo, NY 14260-3000, USA and ⁷Laboratory of Theoretical and Computational Chemistry, Institute of Theoretical Chemistry, Jilin University, 130023 Changchun, PR China

Correspondence: Jing-yao Liu (lly121@jlu.edu.cn) or Mao-sheng Miao (maosheng.miao@csun.edu)

Received: 23 January 2019 Accepted: 20 June 2019

Published online: 11 July 2019

nonhexagonal rings in the graphene lattice does not deteriorate the thermal stability dramatically. And many new exciting properties, such as negative Poisson's ratios (NPR), are obtained. The adsorption of Li atoms to the graphene lattice is also enhanced, which is very important for the performance of rechargeable Li batteries. These results suggest that the rational introduction of structural defects into graphene can be a powerful tool to tailor its local properties and to achieve new functionalities.

RESULTS AND DISCUSSIONS

Figure 1a, b illustrates the strictly planar structure of perfect graphene and the structure of one graphene allotrope that we constructed, respectively. Based on the structural characteristics, we name these constructed graphene allotropes as "egg-tray graphenes". These 2D carbon allotropes are constructed by carefully combining the pentagon and heptagon defects in graphene. It is known that one pentagon in the network of graphene will form a carbon nanocone and one heptagon surrounded by hexagons will form a sheet fragment that curves up in one direction and curves down in the other (Fig. 2a). These characteristics render the pentagon and heptagon surrounded by hexagons as an extreme (maximum/minimum) point and a saddle point in the egg-tray graphene, respectively. However, due to the constraint of the topology, the number of the extreme points (pentagons) should be equal to the number of the saddle points (heptagons), and these critical points need to be arranged evenly. As a general rule, two maxima (or minima) need to be separated by a minimum (maximum) or a saddle point. When combined with 2D symmetry groups, these rules will allow us to construct a number of egg-tray graphenes. Figure 2b, c exhibits two sets of defect arrangements matching the tetragonal and hexagonal symmetry, respectively. In these two topological graphs, the "⊕" stands for the maximum point, the "⊖" stands for the minimum point, and the "⋈" stands for the saddle point. The arrow illustrates the direction of the gradient. The pentagonal nanosheet, composed of one pentagon and five hexagons around it, is used to create the maximum point "⊕" in the topological graphs when the central pentagon is on the top side (the pentagon is filled in green in Fig. 2a), and also the minimum point "⊖" if it is flipped by 180° (the pentagon is filled in yellow in Fig. 2a). The heptagonal nanosheet, composed of one heptagon (shown as red in Fig. 2a) and seven hexagons around it, is used to create the saddle point to connect the maximum and minimum points. Altogether, these two kinds of nanosheets are used as building blocks and are

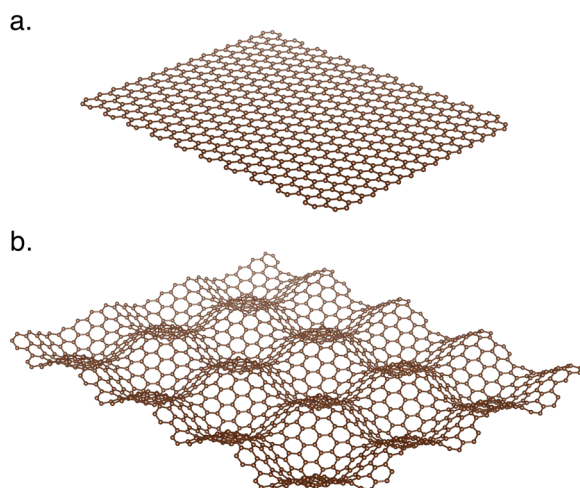


Fig. 1 Optimized structures of graphene and an egg-tray graphene. **a** Two-dimensional structure of pristine graphene. **b** Two-dimensional structure of egg-tray graphene T₁₋₉

arranged according to the topological graphs to build various "egg-tray graphenes". By changing the relative positions of these nanosheets, we can obtain more than one allotrope satisfying the same topological structure.

The top and side views of the optimized atomic configurations of the six smallest egg-tray graphenes are shown in Fig. 2d–i. The egg-tray graphenes were denoted as T/H_{*n*} (*n* = 1, 2, 3, and 4), in which T or H represents tetragonal or hexagonal patterns, and *n* is the serial number for these structures that are sorted by the size of the unit cell. Using the coloring scheme introduced in Fig. 2a, the pentagons in the center of nanocones with convex and concave surfaces are filled with green and yellow, respectively, and the heptagons are filled with red. The top-down views in Fig. 2d–i illustrate that all the nonhexagonal rings are surrounded by hexagons and are separated from each other. Each unit cell of these structures contains only two pentagons and two heptagons, which is determined by the topological graphs. On the other hand, the number of hexagons present depends on the size of the unit cell as shown in Table 1. The presence of pentagons and heptagons in the lattice causes the carbon surface to pucker and curve. Therefore, a thickness ranging from 1.57 to 2.81 Å was observed for these egg-tray graphenes, as illustrated in the side views in Fig. 2d–i.

In the structure of T₁ shown in Fig. 2d, the presence of alternating pentagons and heptagons along the *a* and *b* lattice vectors forms two kinds of narrow nanoribbons. Along either direction, the neighboring narrow nanoribbons are connected by a distorted zigzag or armchair graphene nanoribbon (GNR). Therefore, by modulating the width of the connecting GNRs, the distances between neighboring pentagons and heptagons can be controlled. Importantly, however, the resulting structures still have the same topological pattern. In Fig. S1, the optimized geometries of the expanded T₁ sheet are illustrated. The expanded parts along *a* and *b* are filled by purple and lilac, respectively. As shown in Table S1, this expansion increases the number of hexagons in the unit cell. The amplitude of the carbon nanocones also increases, therefore these expanded T₁ structures are thicker as compared with the original T₁. The distances between neighboring pentagons and heptagons in the unit cells of T₂, H₁, H₂, H₃, and H₄ can also be expanded using the same method, thereby yielding more egg-tray graphenes.

The thermodynamic stability of egg-tray graphenes is investigated by calculating the total energies. As listed in Tables 1 and S1, the egg-tray graphenes are only 0.093–0.32 eV/carbon atom higher in energy than graphene. The energy of these allotropes strongly depends on the amplitude of their curves, which in turn are determined by the number of pentagon and heptagon defects. Allotropes with a larger amount of defects exhibit more curves with a smaller amplitude, and their structures differ more from that of graphene. This usually results in higher energy. As shown in Fig. 3, the energetic stability of egg-tray graphenes changes as a function of the percentage of defects (pentagons and heptagons). T₁₋₉ has the lowest percentage of defects (7%) and also shows the lowest energy, which is only 0.093 eV/atom above that of graphene. As a matter of fact, T₁₋₉ is the most stable system among all the reported 2D carbon allotropes that we are aware of, with the exception of graphene (shown in Table S3).

Although the above thermodynamic stability results indicate that the egg-tray graphenes could be made, their synthesis remains a challenging problem. However, in the last decade, a number of bottom-up chemical synthesis methods have been demonstrated for fabricating 2D materials, including graphene and nanoribbons to highly accurate structures. In many of these bottom-up chemical syntheses of nanographenes, precursors containing pentagonal, heptagonal, and octagonal rings have been used. In 2016, Fasel and co-workers²¹ showed that carefully designed phenyl-substituted polycyclic aromatic hydrocarbons can be used for the rational fabrication of five-membered rings in

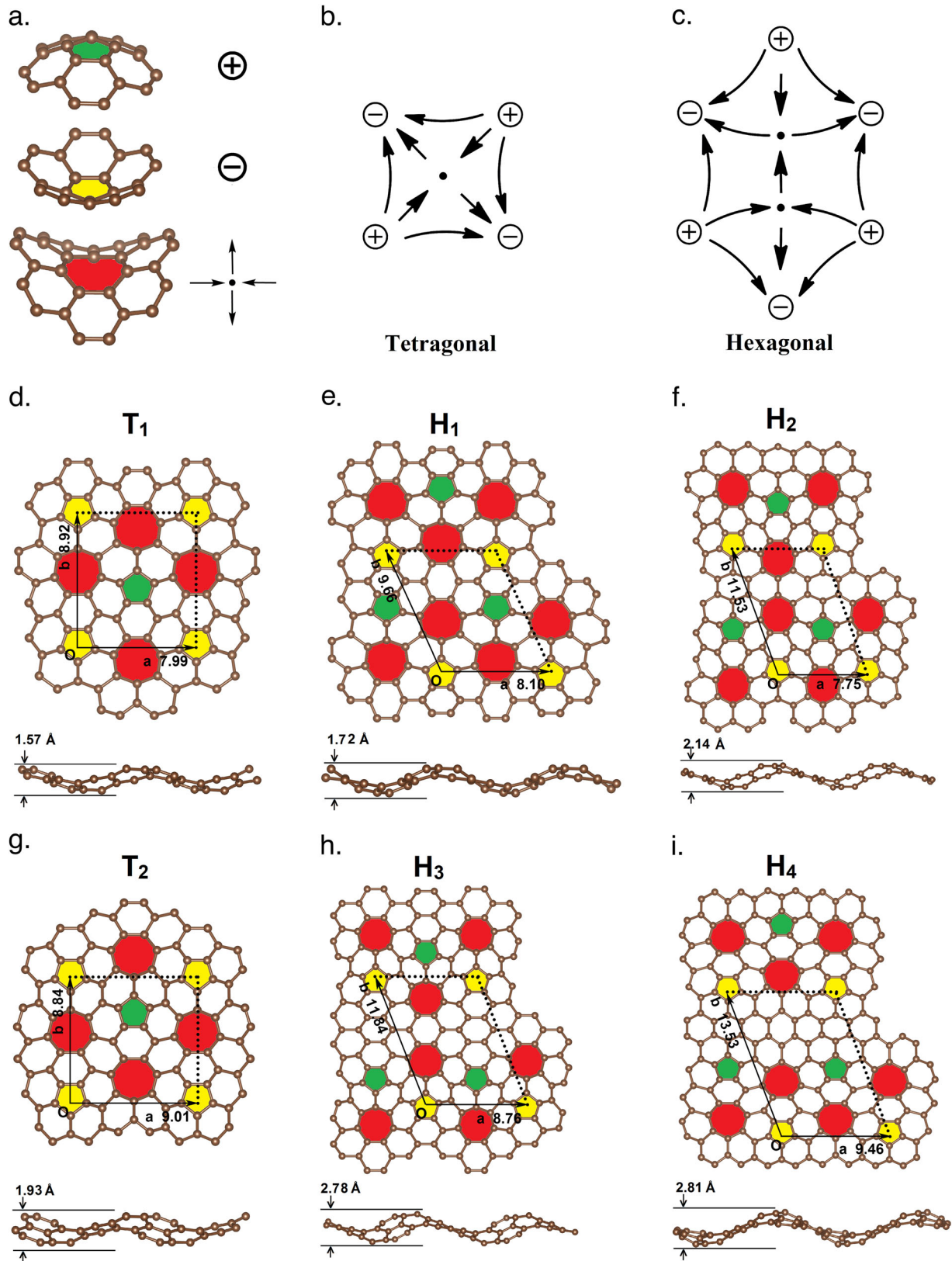


Fig. 2 Schematic illustration of the construction of egg-tray graphenes and the obtained optimized structures. **a** Green and yellow pentagons surrounded by five hexagons denote the maximum and the minimum points, whereas one heptagon surrounded by seven hexagons denotes a saddle point in the topological graphs. **b, c** Tetragonal and hexagonal topological graphs. **d–i** Top and side views of the optimized structures of egg-tray graphenes T_1 , T_2 , H_1 , H_2 , H_3 , and H_4 . Their unit cells are marked by the black lines, and the lattice parameter is given in Angstrom (Å). Brown balls represent carbon atoms

Table 1. Summary of the total number of carbon atoms, 5-, 6-, and 7-membered rings per unit cell, lattice constants a , b and γ , $\Delta E/\text{Carbon}$ (eV, the energy difference between the egg-tray graphene and pristine graphene), and the band gaps (eV) at the PBE and HSE levels of theory for each egg-tray graphene shown in Fig. 2

| System | No. of C atoms | 5 ring | 6 ring | 7 ring | a (Å) | b (Å) | γ (°) | $\Delta E/\text{Carbon}$ | Gap (PBE) | Gap (HSE) |
|----------------|----------------|--------|--------|--------|---------|---------|--------------|--------------------------|-----------|-----------|
| T ₁ | 28 | 2 | 10 | 2 | 7.99 | 8.92 | 90.00 | 0.24 | 0.51 | 0.77 |
| T ₂ | 32 | 2 | 12 | 2 | 9.01 | 8.84 | 90.00 | 0.24 | 0.22 | 0.40 |
| H ₁ | 28 | 2 | 10 | 2 | 8.10 | 9.66 | 114.73 | 0.32 | 0.32 | 0.58 |
| H ₂ | 34 | 2 | 13 | 2 | 7.75 | 11.53 | 109.63 | 0.24 | 0.69 | 0.98 |
| H ₃ | 40 | 2 | 16 | 2 | 8.76 | 11.84 | 111.69 | 0.21 | 0.43 | 0.64 |
| H ₄ | 48 | 2 | 20 | 2 | 9.46 | 13.53 | 110.45 | 0.23 | 0.00 | 0.00 |

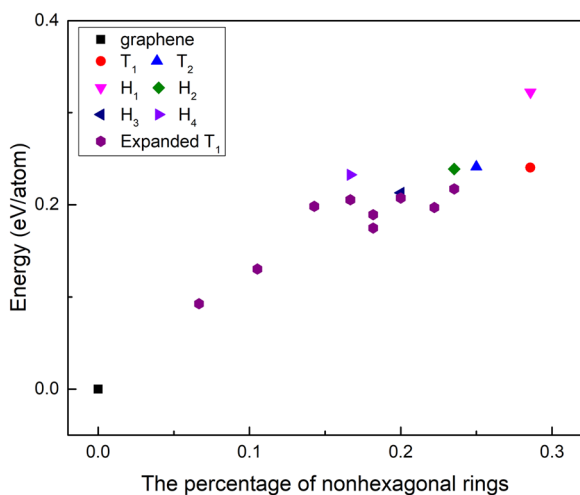


Fig. 3 The correlation between $\Delta E/\text{Carbon}$ (the energy difference between the egg-tray graphene and pristine graphene) and the ratio of defect rings (pentagons and heptagons) to polygons (pentagons, hexagons, and heptagons) for egg-tray graphenes, i.e., the number of defect rings/number of all polygon rings

the bottom-up synthesis of carbon-based nanomaterials. Itami and co-workers²² successfully obtained a 26-ring $C_{80}H_{30}$ nanographene in one single chemical reaction that incorporates one pentagon and five heptagons embedded in a hexagonal lattice. In 2015, Miao et al.²³ synthesized one saddle-shaped polycyclic arene $C_{70}H_{26}$ containing two heptagons and two pentagons that can serve as segments, or synthetic precursors for some egg-tray graphenes. Our calculations show that egg-tray graphenes are among the most stable carbon allotropes. Once they are fabricated, they can persist. As a matter of fact, many allotropes that are much higher in energy such as graphdiyne,²⁴ a C_{20} cage,²⁵ and the smallest carbon nanotube²⁶ (0.77, 1.14, and 1.15 eV/Carbon less stable than graphene, respectively) have been synthesized. Our calculation results and recent experimental studies strongly suggest that the proposed egg-tray graphenes could be fabricated via bottom-up chemical synthesis methods and they can remain stable once they are made.

Moreover, the thermal stability of egg-tray graphenes were examined by performing first-principles molecular dynamics (FPMD) simulations using a canonical (NVT) ensemble. A 2×2 supercell was used for each egg-tray graphene to reduce the constraint of periodic boundary conditions (PBC). FPMD simulations for 4 ps that contained 4000 MD steps at 1000 K did not show any structural reconstruction for any of the egg-tray graphenes, implying that they can withstand temperatures as high as 1000 K. Snapshots of the equilibrium structures of the egg-

tray graphenes at the end of the FPMD simulations are shown in Fig. S2. The dynamic stability of egg-tray graphenes were studied for two selected structures, T₁ and T₂, by calculating their phonon spectra. The obtained results are presented in Fig. S5. The absence of imaginary modes in the entire Brillouin zone confirms that these egg-tray graphenes are also dynamically stable. Most of the other egg-tray graphenes have lower symmetries and larger unit cells, making the calculation of their phonon spectra extremely challenging. On the other hand, if a dynamic instability that is caused by restraining the unit cell and the symmetry exists, it can be removed by relaxing the positions of the carbon atoms in an enlarged unit cell that is usually doubled along the direction of the imaginary phonon modes. Such relaxations usually result in a small energy change and are unlikely to influence the number and the positions of the pentagons and heptagons in the egg-tray graphene, i.e., they are unlikely to change the topology of the structure.

Next, the electronic structures of these egg-tray graphenes were studied. Figure 4 plots the Perdew–Burke–Ernzerhof (PBE) densities of states (DOS), as well as the band structures of T₁, T₂, H₁, H₂, H₃, and H₄ along the high-symmetry lines of the first Brillouin zone. T₁, H₁, and H₃ are semiconductors with direct band gaps of 0.51, 0.32, and 0.43 eV, and their valence band maximum (VBM) and conduction band minimum (CBM) are located at the Y, Y, and Γ points, respectively. T₂ and H₂ are semiconductors with indirect band gaps of 0.22 and 0.69 eV, respectively. The VBM of T₂ is located at Y and its CBM between Γ and M. The VBM of H₂ is located between the Y and Γ points and its CBM is at the Y point. In the band structure of H₄, the VBM and CBM meet at a single point that is located slightly below the Fermi level. The DOS is not zero at the Fermi level, but it is small. This unique feature results in the self-doping of H₄. Considering that the PBE functional always underestimates the band gaps, we also used the screened Heyd–Scuseria–Ernzerhof (HSE) functional to calculate the band structures of the egg-tray graphenes. We found that the band gaps of the five semiconductors were enlarged to 0.40–0.98 eV as listed in Table 1. For H₄, on the other hand, the dispersion of the valence bands and conduction bands around the Fermi level calculated with PBE and HSE is very similar. We can confirm that H₄ is truly gapless.

The PBE band structures and DOS of the expanded T₁ structures are illustrated in Fig. S3. Four direct band gap semiconductors with gaps of 0.063–0.56 eV were obtained. Their VBM and CBM are located at the Γ and Y high-symmetry points, or on the high-symmetry line joining Γ with M. The other five expanded T₁ structures are semi-metals with their VBM and CBM meeting at the Fermi level. This results in a DOS of zero at the Fermi level. Their meeting points are located between two high-symmetry points rather than on a high-symmetry point as for graphene. As shown in Fig. S4, the calculated three-dimensional bands formed by the valence and conduction bands in the vicinity of these meeting points elaborate that these meeting points are Dirac points. The Dirac points of T₁-4, T₁-5, T₁-7, and T₁-9 are located between Y and

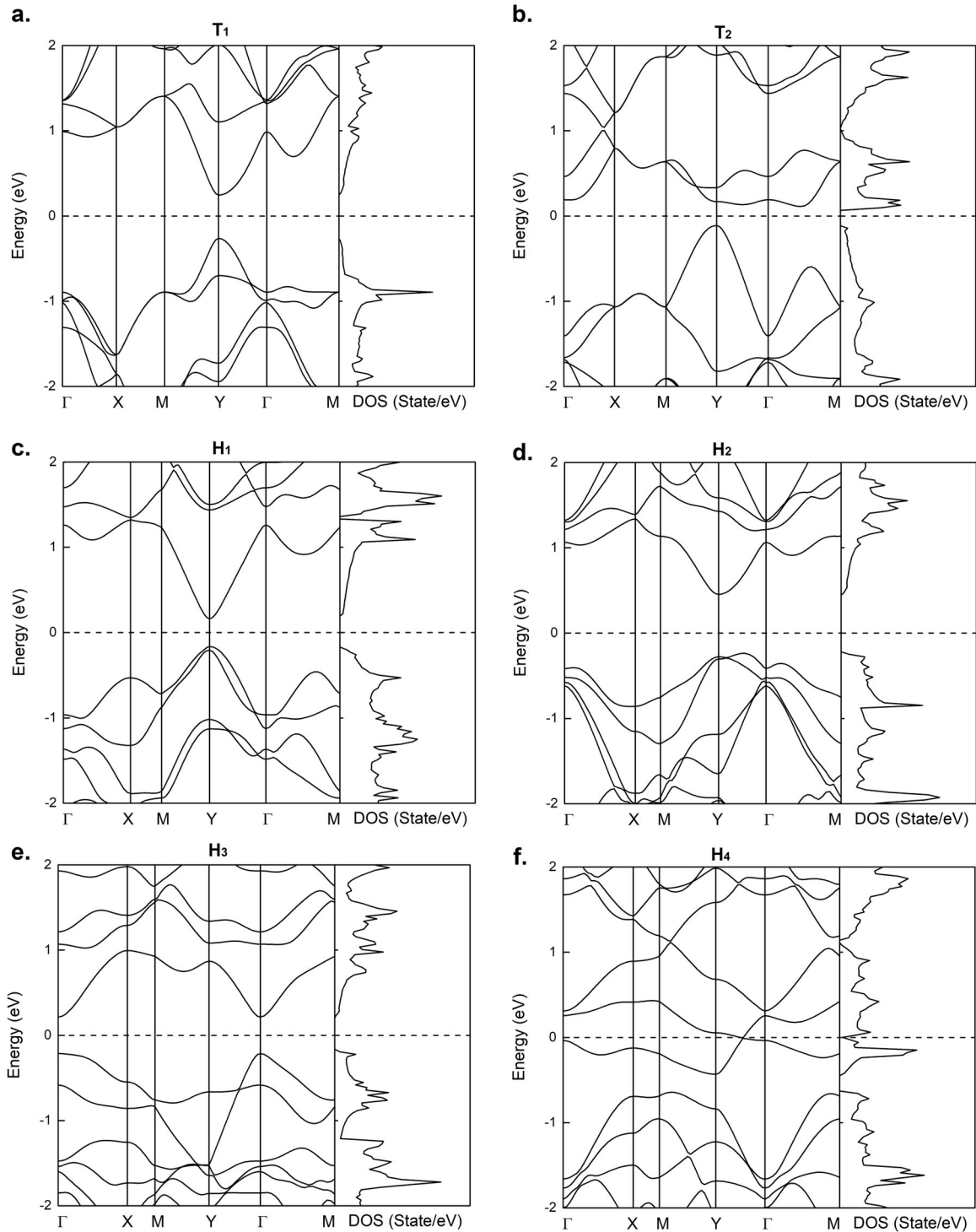


Fig. 4 The PBE band structures and DOS of egg-tray graphenes. **a** T_1 , **b** T_2 , **c** H_1 , **d** H_2 , **e** H_3 , and **f** H_4 . The Fermi levels are shown by black dashed lines

Γ , while the Dirac point of T_1 -8 is located between Γ and X. The band gaps of the semiconductors are enlarged to 0.10–0.80 eV by the HSE hybrid functional, while the gapless properties of the semi-metals are confirmed. As discussed above, T_1 is a semiconductor with a direct band gap of 0.51 eV. By modulating the distances between the neighboring defects, stable graphene allotropes with various electronic properties can be obtained. This provides a systematic way of making 2D carbon allotropes with various electronic structures.

The mechanical properties of the egg-tray graphenes were also investigated by calculating the elastic constants. Our calculated elastic constants of graphene were $C_{11} = C_{22} = 352.19$ N/m and $C_{12} = C_{21} = 61.75$ N/m, which are consistent with the previous experimental²⁷ and theoretical²⁸ results. The computed elastic constants of the egg-tray graphenes are listed in Table 2. Clearly, they all meet the mechanical stability criteria for a 2D sheet ($C_{11}C_{22} - C_{12}^2 > 0, C_{66} > 0$). Their 2D Young's modules, Y_{a_r} , Y_{b_r} , and Poisson's ratios, ν_{a_r} , ν_{b_r} , along the a and b directions are calculated

Table 2. Summary of the elastic constants (J m^{-2}) C_{11} , C_{22} , C_{12} , and C_{66} , the 2D Young's modulus (N m^{-1}), and the Poisson's ratios along the a and b directions, respectively, for each egg-tray graphene

| System | C_{11} | C_{22} | C_{12} | C_{66} | Y_a | Y_b | ν_a | ν_b |
|--------|----------|----------|----------|----------|--------|--------|---------|---------|
| T_1 | 144.23 | 143.08 | -24.45 | 126.50 | 140.05 | 138.94 | -0.17 | -0.17 |
| T_2 | 102.20 | 174.78 | -16.05 | 116.82 | 100.73 | 172.26 | -0.09 | -0.16 |
| H_1 | 247.82 | 93.38 | -15.86 | 101.40 | 245.13 | 92.36 | -0.17 | -0.06 |
| H_2 | 175.96 | 81.69 | -11.66 | 110.10 | 174.29 | 80.92 | -0.14 | -0.07 |
| H_3 | 159.62 | 116.11 | 1.35 | 99.12 | 159.60 | 116.10 | 0.01 | 0.01 |
| H_4 | 225.94 | 55.17 | -11.81 | 92.97 | 223.41 | 54.56 | -0.21 | -0.05 |

using the following equations, respectively:

$$Y_a = \frac{C_{11}C_{22} - C_{12}^2}{C_{22}} \quad \text{and} \quad Y_b = \frac{C_{11}C_{22} - C_{12}^2}{C_{11}}, \quad (1)$$

$$\nu_a = \frac{C_{12}}{C_{22}} \quad \text{and} \quad \nu_b = \frac{C_{12}}{C_{11}} \quad (2)$$

As listed in Table 2, their Young's moduli lie in the range from 80.92 to 245.13 N/m, which is smaller than that of graphene (331.63 N/m), but larger than that of phosphorene (25.50 N/m, 91.61 N/m). Their two Young's moduli Y_a and Y_b are not equal, which means that the egg-tray graphenes are mechanically anisotropic. We also note that T_1 , T_2 , H_1 , H_2 , and H_4 have unusual NPR, which originates from the negative C_{12} . The NPR means that the material can be stretched or compressed in both the a and b directions at the same time, meaning that it exhibits auxetic behavior. Auxetic materials usually have excellent mechanical properties compared with conventional materials. The auxetic behavior of egg-tray graphenes can be explained via the auxetic egg-rack mechanism.²⁹ All these results demonstrate that the egg-tray graphenes should have good mechanical properties.

Finally, we use the T_1 and T_2 structures as an example to investigate the adsorption and diffusion of Li atoms on the egg-tray graphenes. As reported in a recent work on Li adsorption on graphene,³⁰ Li atoms prefer to adsorb to the centers of polygons, rather than the top or bridge sites. The same is true for egg-tray graphenes. The possible Li adsorption sites on graphene, T_1 and T_2 are illustrated in Fig. 5a–c, respectively. As listed in Table S2, the binding energy of one Li atom adsorbed on graphene is 1.20 eV, which is consistent with previously reported values.^{30,31} The binding energies of one Li atom adsorbed to different sites on the T_1 and T_2 sheets are in the range of 1.50–1.61 eV and 1.61–1.71 eV, respectively, which means that both T_1 and T_2 have higher binding affinities to Li than graphene. The most stable adsorption site on T_1 is hex3, and for T_2 the most stable adsorption site is hep1. It is noteworthy that the adsorption of one Li atom on hexagons in T_1 and T_2 are more favorable than on graphene, indicating that the presence of defects such as pentagons and heptagons in T_1 and T_2 enhance the binding affinity compared with graphene. It has been reported previously^{31,32} that the presence of carbon vacancies in graphene could increase the binding strength of Li to the carbon surface.

We also considered the adsorption of a second Li atom on the neighboring polygons of the most stable adsorption sites in graphene and the egg-tray graphenes (T_1 and T_2). We assumed that the first Li atom is located at the most stable adsorption site. As shown in Fig. 5d–f, the binding energy of two Li atoms on neighboring hexagons in graphene is 0.27 eV smaller than that of the first Li atom adsorbing on graphene, which can be attributed to the Coulombic repulsion between the neighboring electro-positive Li atoms after donating electrons to graphene. The adsorption of two Li atoms on neighboring polygons in T_1 and T_2 is also weaker than that of a single Li atom, but it is still stronger than the adsorption of one single Li to graphene. The higher

binding energies of Li atoms adsorbing to T_1 and T_2 suggest that egg-tray graphenes may possess a larger Li/C ratio than graphene, which is important for the performance of rechargeable Li batteries.

The diffusion behavior of Li ions is important for the performance of Li-ion batteries. The Li diffusion processes on both T_1 and T_2 surfaces are investigated using the climbing-image nudged elastic band method.³³ A total of 2×2 supercells of T_1 and T_2 containing 112 and 128 carbon atoms, respectively, were employed in these calculations to reduce the artificial interaction between adjacent image cells. As shown in Fig. 5g, i, three possible migration pathways between the neighboring lowest-energy adsorption sites (hex3 site in T_1 and hep1 site in T_2) for both T_1 and T_2 were considered, respectively. Selected positions of Li ion along these pathways are indicated by red (Path1), blue (Path2), and green (Path3), respectively. The Li ion could diffuse along the whole surfaces of T_1 and T_2 by combining different pathways since the barrier crossing the carbon polygons are quite similar. As shown in Fig. 5h, j, the calculated diffusion barriers along the three pathways are plotted, which are 0.268, 0.388, and 0.273 eV for T_1 , and 0.406, 0.439, and 0.272 eV for T_2 , respectively. These diffusion barriers are comparable with the Li diffusion barriers for graphene (0.277 eV),³⁴ graphene with grain boundaries (0.245–0.331 eV)³⁵ and different edge modified one-dimensional graphene (0.132–0.285),³⁶ but smaller than that of graphite (0.47 eV),³⁷ showing no diffusion problem for this family of graphene allotropes while used as anode materials.

In summary, we proposed a strategy to topologically arrange defect structures in a graphene lattice. A series of graphene allotropes with both positively and negatively curved carbon surfaces are constructed and studied by first-principles calculations based on density functional theory (DFT). The egg-tray graphenes are energetically very stable compared with other 2D carbon allotropes. One of them is only 0.093 eV/Carbon higher in energy than graphene, which makes it the most stable graphene allotrope ever reported. The electronic structures of the egg-tray graphenes vary greatly ranging from semimetallic to semiconducting with a tunable gap. Some egg-tray graphenes are found to have unusual NPR. Due to the larger Li/C ratio than that found in graphene and the moderate Li diffusion barriers, egg-tray graphenes could be used as anode materials. Therefore, egg-tray graphenes could have wide potential applications in future electronics and mechanics, in the likely event that they are synthesized.

METHODS

Our calculations were performed using DFT as implemented in the Vienna Ab Initio Simulation package.³⁸ The projector augmented wave³⁹ approach was used to describe the ionic potential, and the generalized gradient approximation (GGA) of PBE⁴⁰ was employed to describe the exchange–correlation interactions. PBC were applied, and a vacuum space of 20 Å along the (001) direction was employed in the computations to prevent interactions between neighboring layers. The Monkhorst–Pack scheme⁴¹ with a $7 \times 7 \times 1$ k -mesh was used to sample the first Brillouin

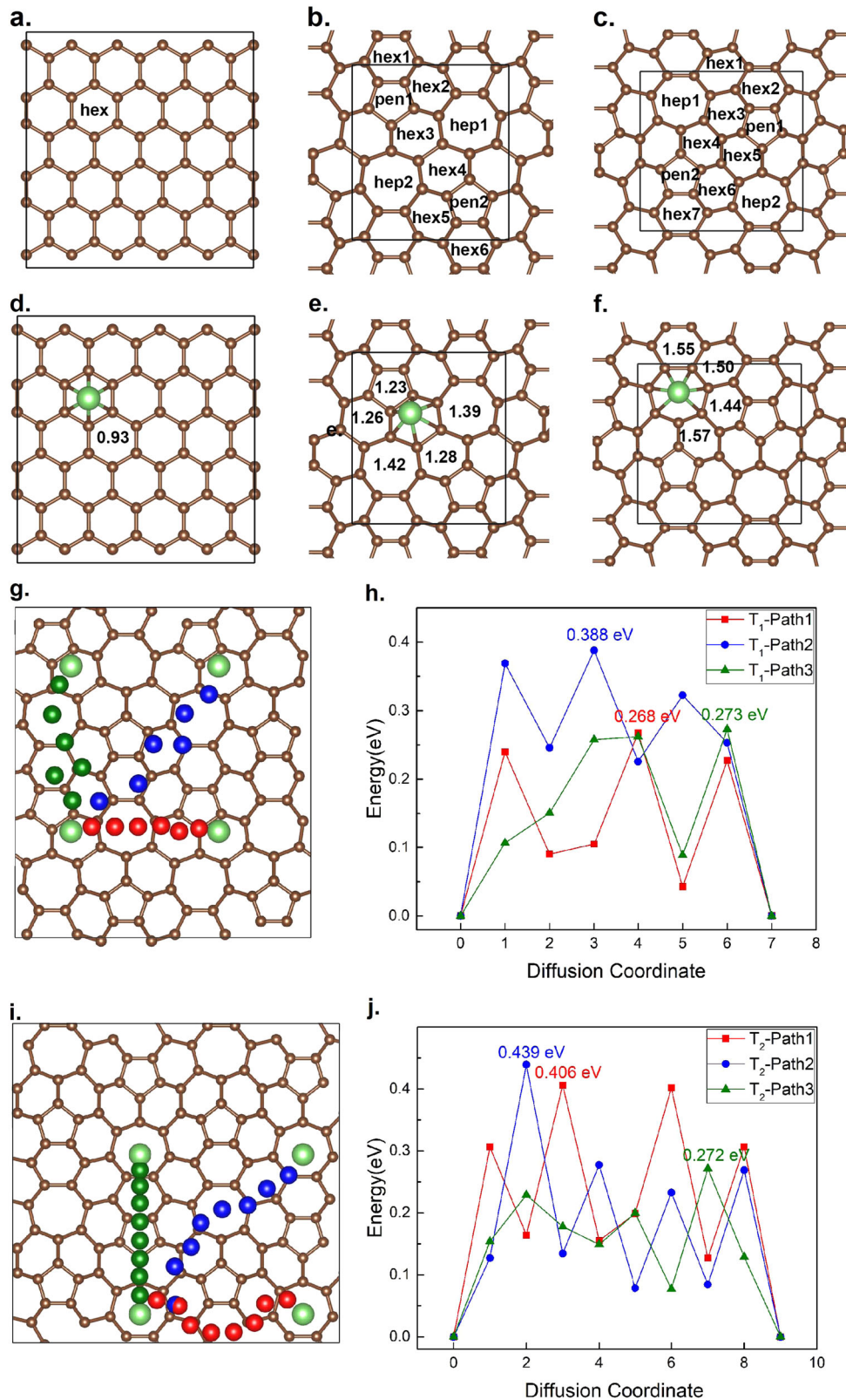


Fig. 5 Adsorption and diffusion of Li on the surfaces of graphene and egg-tray graphene. **a–c** The considered Li adsorption sites on graphene, T₁ and T₂. **d–f** Top views of the configurations for one single Li atom adsorbed at the most stable adsorption site on graphene, T₁ and T₂. “hex” indicates the center of a hexagon, “pen” the center of a pentagon, and “hep” the center of a heptagon. The numbers indicate the binding energies (in the unit of eV/Li) of the two Li atoms adsorbed on the neighboring polygons. The first Li atom is fixed onto the most stable adsorption site and the second Li is placed on one of the neighboring polygon centers for which the binding energy of the pair is shown. **g, i** Diffusion pathways of Li ion on T₁ and T₂. **h, j** The corresponding diffusion barriers for the pathways on T₁ and T₂. Brown balls represent carbon atoms; light green balls represent Li atoms

zone. The energy cutoff for the calculations was set to 900 eV. The convergence criteria adopted were 1×10^{-5} eV/atom for the self-consistent total energy, 0.01 eV/Å for the force component on each atom and 0.01 eV/Å³ for the stress tensor component on the cell in the structure optimizations. The conjugated gradient method was used to optimize the structures. Because GGA functionals always underestimate the band gaps of semiconductors, both the HSE⁴² hybrid functional and the PBE functional were used to calculate the band structures and DOS.

DATA AVAILABILITY

All data generated and/or analyzed during this study are included in this published article and its supplementary information file.

ACKNOWLEDGEMENTS

Calculations are performed on NSF-funded XSEDE resources (TG-DMR130005) especially on Stampede cluster ran by TACC. This research is also supported by the National Natural Science Foundation of China (Grants no. 21773083). E.Z. acknowledges the NSF (DMR-1827815) for financial support. W.L. acknowledges the Scientific Research and Developed Fund of the Zhejiang A & F University (No. 2019FR006) for financial support.

AUTHOR CONTRIBUTIONS

W.L. and M.M. conceived the research; W.L. and L.Z. performed the calculations and analyzed the data; W.L. wrote the manuscript; M.M., E.Z., J.X., Y.Z., H.L. and J.L. helped to revise the manuscript. All authors discussed and commented on the manuscript.

ADDITIONAL INFORMATION

Supplementary information accompanies the paper on the *npj Computational Materials* website (<https://doi.org/10.1038/s41524-019-0211-2>).

Competing interests: The authors declare no competing interests.

Publisher's note: Springer Nature remains neutral with regard to jurisdictional claims in published maps and institutional affiliations.

REFERENCES

- Novoselov, K. S. et al. Electric field effect in atomically thin carbon films. *Science*. **306**, 666–669 (2004).
- Novoselov, K. S. et al. A roadmap for graphene. *Nature*. **490**, 192–200 (2012).
- Geim, A. K. & Novoselov, K. S. The rise of graphene. *Nat. Mater.* **6**, 183–191 (2007).
- Novoselov, K. S. et al. Room-temperature quantum Hall effect in graphene. *Science*. **315**, 1379–1379 (2007).
- Mayorov, A. S. et al. Micrometer-scale ballistic transport in encapsulated graphene at room temperature. *Nano Lett.* **11**, 2396–2399 (2011).
- Novoselov, K. S. et al. Two-dimensional gas of massless Dirac fermions in graphene. *Nature*. **438**, 197–200 (2005).
- Morozov, S. V. et al. Giant intrinsic carrier mobilities in graphene and its bilayer. *Phys. Rev. Lett.* **100**, 016602 (2008).
- Balandin, A. A. Thermal properties of graphene and nanostructured carbon materials. *Nat. Mater.* **10**, 569–581 (2011).
- Haskins, J. et al. Control of thermal and electronic transport in defect-engineered graphene nanoribbons. *ACS Nano*. **5**, 3779–3787 (2011).
- Tsen, A. W. et al. Tailoring electrical transport across grain boundaries in polycrystalline graphene. *Science*. **336**, 1143–1146 (2012).
- Banhart, F., Kotakoski, J. & Krasheninnikov, A. V. Structural defects in graphene. *ACS Nano*. **5**, 26–41 (2011).
- Vicarelli, L., Heerema, S. J., Dekker, C. & Zandbergen, H. W. Controlling defects in graphene for optimizing the electrical properties of graphene nanodevices. *ACS Nano*. **9**, 3428–3435 (2015).
- Stone, A. J. & Wales, D. J. Theoretical studies of icosahedral C₆₀ and some related species. *Chem. Phys. Lett.* **128**, 501–503 (1986).
- Liu, M. et al. Graphene-like nanoribbons periodically embedded with four- and eight-membered rings. *Nat. Commun.* **8**, 14924 (2017).
- Grima, J. N. et al. Tailoring graphene to achieve negative Poisson's ratio properties. *Adv. Mater.* **27**, 1455–1459 (2015).

- Lusk, M. T. & Carr, L. D. Nanoengineering defect structures on graphene. *Phys. Rev. Lett.* **100**, 175503 (2008).
- Yang, N., Zhang, G. & Li, B. Carbon nanocone: a promising thermal rectifier. *Appl. Phys. Lett.* **93**, 243111 (2008).
- Baei, M. T., Peyghan, A. A. & Bagheri, Z. Carbon nanocone as an ammonia sensor: DFT studies. *Struct. Chem.* **24**, 1099–1103 (2012).
- Vessally, E. et al. Carbon nanocone as an electronic sensor for HCl gas: quantum chemical analysis. *Vacuum*. **134**, 40–47 (2016).
- Odkhuu, D. et al. Negatively curved carbon as the anode for lithium ion batteries. *Carbon*. **66**, 39–47 (2014).
- Liu, J. et al. Building pentagons into graphenic structures by on-surface polymerization and aromatic cyclodehydrogenation of phenyl-substituted polycyclic aromatic hydrocarbons. *J. Phys. Chem. C*. **120**, 17588–17593 (2016).
- Kawasumi, K. et al. A grossly warped nanographene and the consequences of multiple odd-membered-ring defects. *Nat. Chem.* **5**, 739–744 (2013).
- Cheung, K. Y., Xu, X. & Miao, Q. Aromatic saddles containing two heptagons. *J. Am. Chem. Soc.* **137**, 3910–3914 (2015).
- Li, G. et al. Architecture of graphdiyne nanoscale films. *Chem. Commun.* **46**, 3256–3258 (2010).
- Prinzbach, H. et al. Gas-phase production and photoelectron spectroscopy of the smallest fullerene, C₂₀. *Nature*. **407**, 60–63 (2000).
- Zhao, X. et al. Smallest carbon nanotube is 3 Å in diameter. *Phys. Rev. Lett.* **92**, 125502 (2004).
- Lee, C., Wei, X., Kysar, J. W. & Hone, J. Measurement of the elastic properties and intrinsic strength of monolayer graphene. *Science*. **321**, 385–388 (2008).
- Andrew, R. C., Mapasha, R. E., Ukpogon, A. M. & Chetty, N. Mechanical properties of graphene and boronitrene. *Phys. Rev. B*. **85**, 125428 (2012).
- Grima, J. N., Williams, J. J. & Evans, K. E. Networked calix[4]arene polymers with unusual mechanical properties. *Chem. Commun.* **7**, 4065–4067 (2005).
- Chan, K. T., Neaton, J. B. & Cohen, M. L. First-principles study of metal adatom adsorption on graphene. *Phys. Rev. B*. **77**, 235430 (2008).
- Fan, X., Zheng, W. T. & Kuo, J.-L. Adsorption and diffusion of Li on pristine and defective graphene. *ACS Appl. Mater. Interfaces*. **4**, 2432–2438 (2012).
- Yildirim et al. First-principles analysis of defect-mediated Li adsorption on graphene. *ACS Appl. Mater. Interfaces*. **6**, 21141–21150 (2014).
- Henkelman, G. & Jónsson, H. Improved tangent estimate in the nudged elastic band method for finding minimum energy paths and saddle points. *J. Chem. Phys.* **113**, 9978–9985 (2000).
- Zhou, L.-J., Hou, Z. F. & Wu, L.-M. First-principles study of lithium adsorption and diffusion on graphene with point defects. *J. Phys. Chem. C*. **116**, 21780–21787 (2012).
- Zhou, L.-J., Hou, Z. F., Wu, L.-M. & Zhang, Y.-F. First-principles studies of lithium adsorption and diffusion on graphene with grain boundaries. *J. Phys. Chem. C*. **118**, 28055–28062 (2014).
- Leggesse, E. G., Chen, C.-L. & Jiang, J.-C. Lithium diffusion in graphene and graphite: effect of edge morphology. *Carbon*. **103**, 209–216 (2016).
- Toyoura, K. et al. First-principles approach to chemical diffusion of lithium atoms in a graphite intercalation compound. *Phys. Rev. B*. **78**, 214303 (2008).
- Kresse, G. & Furthmüller, J. Efficient iterative schemes for ab initio total-energy calculations using a plane-wave basis set. *Phys. Rev. B*. **54**, 11169–11186 (1996).
- Blöchl, P. E. Projector augmented-wave method. *Phys. Rev. B*. **50**, 17953–17979 (1994).
- Perdew, J. P., Burke, K. & Ernzerhof, M. Generalized gradient approximation made simple. *Phys. Rev. Lett.* **77**, 3865–3868 (1996).
- Monkhorst, H. J. & Pack, J. D. Special points for Brillouin-zone integrations. *Phys. Rev. B*. **13**, 5188–5192 (1976).
- Heyd, J., Scuseria, G. E. & Ernzerhof, M. Hybrid functionals based on a screened Coulomb potential. *J. Chem. Phys.* **118**, 8207–8215 (2003).



Open Access This article is licensed under a Creative Commons Attribution 4.0 International License, which permits use, sharing, adaptation, distribution and reproduction in any medium or format, as long as you give appropriate credit to the original author(s) and the source, provide a link to the Creative Commons license, and indicate if changes were made. The images or other third party material in this article are included in the article's Creative Commons license, unless indicated otherwise in a credit line to the material. If material is not included in the article's Creative Commons license and your intended use is not permitted by statutory regulation or exceeds the permitted use, you will need to obtain permission directly from the copyright holder. To view a copy of this license, visit <http://creativecommons.org/licenses/by/4.0/>.

© The Author(s) 2019